RSC Advances

ROYAL SOCIETY OF CHEMISTRY

www.rsc.org/advances

- **A table of contents entry**

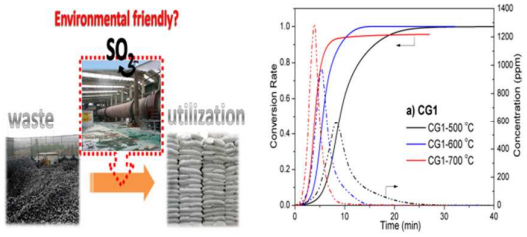

The SO_2 emission behavior of coal gangue during calcination was systematically investigated.

Pyrite Transformation and Sulfur Dioxide Release during Calcination of Coal Gangue

*Yingyi Zhang[1], Xinlei Ge[2], Jinichiro Nakano[3], Lili Liu[1], Xidong Wang[1], Zuotai Zhang[1]**

[1] Beijing Key Laboratory for Solid Waste Utilization and Management and Department of Energy and Resource Engineering, College of Engineering, Peking University, Beijing, 100871, P.R. China

[2] Jiangsu Key Laboratory of Atmospheric Environment Monitoring and Pollution Control, School of Environmental Science and Engineering, Nanjing University of Information Science & Technology, Nanjing 210044, PR China

[3] URS Corp., PO BOX 1959, Albany, OR 97321, USA

*Corresponding author.

Tel.: +86 10 82524880

E-mail address: zuotaizhang@pku.edu.cn (Z.T. Zhang).

ABSTRACT

Calcination is a typical process associated with the utilization of coal gangue. A concern of this procedure is the emission of sulfur dioxide (SO_2). In this work, the behaviors of SO_2 release during coal gangue calcination under air atmosphere were systematically investigated, and

compared to the characteristics of SO_2 evolution from pure pyrite calcination. Results show that although sulfur in coal gangue mainly exists in the form of pyrite, it represents different transformation behaviors from that in pure mineral pyrite. At 500 ^oC, the release rate of SO_2 is significantly higher in coal gangue than in mineral pyrite due to the fact that coal gangue combustion can occur at low temperature which favors the SO_2 release, while at 600 and 700 ^oC they become almost the same. The shrinking core model cannot describe the SO_2 emission profiles in coal gangue, instead, a hybrid 3D diffusion - Jander model is successfully developed in this study.

Keywords: Coal gangue, SO_2 emission, Pyrite, Calcination;

1. Introductions

With increasing environmental and economic burden of waste disposal, utilization of waste material as an alternative for declining fossil fuel and mineral resources has gained considerable interest worldwide. However, attention should be paid to the potential secondary pollution generated during the utilization, as it may constrain the development of the utilization and pose new challenges to the environment protection [1]. Coal gangue is a problematic solid waste discharged from coal mining and beneficiation [2-4]. Substantial quantities of coal gangue were dumped in every coal-producing country, causing a series of environmental problems, such as acid drainage, heavy metals leaching as well as atmospheric pollution [5-7]. In China, there is still about 659 million tons of coal gangue produced each year [8]. As coal gangue has high contents of silica and alumina, it finds application as a substitute for clay in construction industry [9, 10]. The amounts of coal gangue used in construction industry were up to 50 million tons in 2011 in China [8].

Coal gangue utilized in construction industry is generally subjected to calcination process. As coal gangue contains sulfur derived from both coal components and minerals, the emission of SO_2 during calcination is one of the major environmental concerns. With increasing environmental awareness, recently studies have been carried out on the emission of trace elements of coal gangue during combustion and brick making [3, 11, 12]. However, much less is known about the SO_2 emission during calcination of coal gangue. Sulfur in coal gangue can exist in both organic and inorganic forms. The forms of organic sulfur are rarely reported and their amounts are likely small. For inorganic sulfur compounds, pyrite is a frequently observed and abundant inclusion. The SO_2 emission of coal gangue during calcination is expected to be highly related with the transformation behavior of embedded pyrite. As coal gangue contains both combustible matters and large fractions of mineral species, including kaolinite, quartz and calcite, etc, pyrite may interact with those substances during calcination. Thus the embedded pyrite in coal gangue may exhibit a distinct transformation behavior and SO_2 emission profile compared with coal or pyrite individuals. With increasing stringent regulations on pollution emission, investigations regarding the SO_2 formation mechanism and release behavior during coal gangue calcination are imperative and desirable for the sustainable development of coal gangue utilization.

In this work, the SO_2 release behaviors and pyrite transformation of coal gangue were investigated in comparison with pure pyrite. Compared with the widely used thermal analysis method, a tube furnace was employed to achieve the high flow rate and obtain effective gas-solid contact, which is rather close to the practical conditions. Effects of reaction temperatures, the reaction mechanism and kinetics of pyrite transformation in coal gangue during calcination were also discussed.

2. Materials and methods

2.1. Materials

The two coal gangue samples used in the present investigation, denoted as CG1 and CG2, were collected from two centralized coal waste dumps in Shanxi province, China. The samples were crushed and sieved to a particle size less than 150 μm before use. Proximate analysis was carried out by a thermogravimetric analyzer (TGA-701, LECO) and ultimate analysis was performed by an elemental analyzer (vario Macro CHNS, Elementar). Analyses of the total sulfur and sulfur forms were conducted according to the Chinese standards GB/T 214 [13] and GB/T 215 [14] respectively. The chemical compositions were determined by an X-ray fluorescence spectrometer (S4-Explorer, Bruker). A standard mineral pyrite sample (GBW07267, Fe 48.08±0.29 wt %, S 52.72±0.21 wt %) was purchased from Aikong biological technology (Beijing, China), Ltd. The air (purity >99%) used was provided by Qianxi gas company (Beijing, China), Ltd.

2.2. Calcination and emission experiments

The calcination experiments of coal gangue samples and mineral pyrite were carried out using a vertical tube furnace and the release of SO_2 was recorded simultaneously by a flue gas analyzer (Testo pro350, Testo) at regular intervals of 2s. The experimental setup is illustrated in Fig. 1. Both non-isothermal and isothermal experiments were conducted. During the non-isothermal experiments, the samples were placed into the furnace at ambient temperature and heated up to 1200 ^{o}C at a heating rate of 5 ^{o}C/min. During the isothermal experiments, the furnace was first heated up to a constant temperature (500 ^{o}C, 600 ^{o}C and 700 ^{o}C) and then the samples were quickly loaded into the furnace. Coal gangue samples of 250.0 mg and pure pyrite

of 10.0 mg which has an equivalent sulfur content with CG2, were used. The non-isothermal and isothermal measurements were both performed under air atmosphere at a flow rate of 1.2 L/min. To investigate the mineral phase transformation, 200.0 mg pyrite were calcined under the same conditions. A corundum crucible (Tangshan industrial ceramic plant, China) with a depth of 1 cm and a diameter of 6 cm was used, so that all samples can be well distributed within a thin layer to improve the gas-solid contact.

2.3. Thermal analysis

The thermogravimetric (TGA), derivative thermogravimetric (DTG) and differential scanning calorimetric (DSC) curves were measured using a thermal analyzer (Q600SDT, Thermal analysis) with 10 mg sample inside the alumina crucible. The analyses were performed with an air flow rate of 100 ml/min and a linear heating rate of 10 K/min from room temperature to 1200 ^{o}C.

2.4. X-ray diffraction (XRD)

The XRD analyses of coal gangue samples, mineral pyrite and their residues after combustion were run on a Rigaku D/max 2500 PC X-ray diffractometer with Cu Kα radiation (λ = 0.15406 nm) and operating at 40 kV and 100 mA. The scanning range of 2θ was 10-60º with an increment of 0.02º, under the scanning speed of 2º/min.

3. Results and discussion

3.1. Characterization of Coal Gangue

The chemical compositions of CG1 and CG2 are listed in Table 1. It shows that sulfur in coal gangue is predominately in pyritic forms, accounting for 78.8% and 89.0% of the total sulfur mass in CG1 and CG2, respectively. The mass fractions of organic sulfur to total sulfur in coal gangue are relatively low, only 15.2% in CG1 and 7.7% in CG2. The distributions of different types of sulfur in coal gangue are clearly different from those reported in coal. For instance, Gornostayev et al. [15] reported that the fraction of pyritic sulfur varied considerably from 3% to 63% in coals, and organic sulfur could occupy a significant fraction of the total sulfur. This difference might be ascribed to the compositional features of coal gangue, which contains low level of organics but high content of ash. The dominance of pyritic sulfur in coal gangue affirms that pyritic sulfur or pyrite plays a major role in the subsequent SO_2 formation during calcination of coal gangue.

The major mineral phases found in the two coal gangues are kaolinite and quartz, with minor contributions from pyrite, illite and calcite (Fig. 2a). The morphology of pyrite in coal gangue (CG2) is shown in Fig. 2b. It can be seen that pyrite was closely surrounded by aluminosilicate mineral species. In contrast, O'Brien et al. [16] observed that pyrite in coal was mostly dotted in organic maceral or next to silicates. The different distribution of pyrite in coal gangue as well as its mineral components may lead to different SO_2 release behavior compared with coal.

The general thermal properties of coal gangue are shown by the TGA, DTG and DSC curves in Fig. 3. The thermal behavior of pure pyrite is also illustrated as a comparison. Sharp exothermal peaks are observed at 400 ^{o}C to 600 ^{o}C on the DSC curves of coal gangue, accompanied by the dramatic weight loss shown on the TGA curves in the same temperature interval, indicating that the carbon content in coal gangue undergoes combustion in this

temperature range. It is known that kaolinite also received dehydroxylation in 400 ^{o}C to 600 ^{o}C [11, 17]. Therefore, it appears that the exothermal effect caused by coal gangue combustion is dominant, and overweighs the endothermic effect due to kaolinite dehydroxylation. The pure pyrite exhibits a similar behavior, with a dramatic weight loss and significant exothermic effect around 500 ^{o}C. Overall, at 400 ^{o}C to 600 ^{o}C, coal gangue may release low molecular weight volatile chemicals due to uncompleted combustion, H_2O (g) from kaolinite dehydroxylation and SO_2 due to oxidation of pyrite. These gaseous species together may complicate the release behavior of SO_2 in coal gangue.

3.2. SO_2 Release during Calcination of Coal Gangue.

The following equation can be used to describe the conversion of sulfur to SO_2 [18, 19]:

$$x_s(t) = \frac{\int_0^t C_s(t)V(t)dt}{m_s} \qquad (1)$$

where x_s is the conversion rate of sulfur content in sample to SO_2, t is a certain time during the experiment, min, $C_s(t)$ is the concentration of SO_2 in flue gas corresponding to t, μg/L, $V(t)$ is the flow rate of the flue gas, L/min, which is kept constant at 1.2 L/min in this study, m_s is the mass of total sulfur in the sample, μg.

The SO_2 release and conversion profiles of two coal gangue samples (CG1 and CG2) up to 1200 ^{o}C are presented in Fig. 4, along with the results of pure pyrite. It can be seen that both the two coal gangue samples release SO_2 in advance of pure pyrite. CG1 and CG2 start to release SO_2 at 400 ^{o}C and 450 ^{o}C respectively, while only above 500 ^{o}C, measurable SO_2 release is observed for pure pyrite. These results are in accord with the thermal behaviors observed in DSC curves of Fig. 3. In Fig. 3, both the starting and peak temperature of the exothermic peak of pure

pyrite is higher than that of coal gangue. The starting temperature of SO_2 release from coal gangue is lower than that of pure pyrite, consistent with the observed results in a high sulfide containing shale by Hansen et al. [18], from which the shale-pyrite mixture released SO_2 at a lower temperature than pure pyrite as well. Considering that both shale [18] and coal gangue experience combustion and release heat at lower temperatures than that of pure pyrite, the advance release of SO_2 may result from the elevated local temperature of embedded pyrite in coal gangue due to the heat released from the combustion. It can be seen from DSC curves of coal gangue (shown in Fig. 3) that coal gangue indeed has exothermal effect at 400 ^oC. Meanwhile, the conversion profiles in Fig. 4 show that the sulfur in CG1 was almost completely converted to SO_2, while CG2 and pyrite failed to achieve 100% conversion due to the formation of sulfate in residue ash. Both the relatively high content of alkali metal oxides in CG2 and the exposure to abundant oxygen for pyrite can contribute to the formation of sulfate.

The effects of temperature on the release profiles and conversion rates of sulfur in coal gangue are illustrated in Fig. 5a-b. It can be seen that concentration profiles of SO_2 become narrower and higher as the temperature rises and their peaks appear earlier. The two samples show overall similar behaviors. In both samples, the increase of the slope of conversion curve is relatively significant as the temperature rises from 500 ^oC to 600 ^oC, and becomes small when the temperature further rises to 700 ^oC. The slope of conversion curve of CG1 at 500 ^oC is higher than that of CG2 at 500 ^oC. In addition, the sulfur in CG1 reaches complete conversion to SO_2 in 30 minutes at 500 ^oC while the release of SO_2 in CG2 is still in progress. Given that CG1 actually contains more sulfur than CG2, this result reveals a much higher reaction rate of sulfur transformation in CG1 than that in CG2. At 600 ^oC, the sulfur in coal gangue was entirely converted to SO_2 in both CG1 and CG2 while at 700 ^oC, they both failed to reach 100%

conversion. It may be because of the formation of sulfate which retained part of sulfur in residue ash. CG2 has a significant content of calcite. The calcite decomposes to lime and carbon dioxide at 700 ^{o}C (shown in Fig. 3), which favors the formation of calcium sulfate in CG2.

By comparison, the results for pure pyrite under the same experimental conditions are shown in Fig. 5c. It is noted that the SO_2 release behavior of pyrite is largely different with that of coal gangue at 500 ^{o}C. In comparison with coal gangue, the release rate of SO_2 from pyrite is much slower at 500 ^{o}C. The lag further becomes small at 600 ^{o}C while at 700 ^{o}C, it becomes almost the same with that of coal gangue. Conversion of pyrite into SO_2 at 500 ^{o}C proceeds slowly and reaches only 58% even after a long reaction time of 170 min, and a 100% conversion can only be achieved when the temperatures are increased to 600 ^{o}C and higher.

In addition, it is interesting that we observed a thin white layer adhered to the wall of the cooling zone of the tube after many runs of experiments on coal gangue. By dissolving it into 1 mL deionized water, the pH value of the solution was measured at ~3.0. This result indicates that some acidic species can evaporate during calcination of coal gangue. These acidic materials may be formed by the interactions of SO_2 with other organic substances or volatile elements, such as Na. Moreover, since kaolinite can dehydroxylate at 500 - 700 ^{o}C, the H_2O released may help to dissolve and the condensation the tube wall when cooled down. The XRD pattern of the collected powder, shown in Fig. SI1, confirmed the generation of sulfates and hydrates.

3.3. Transformation of Pyrite

As aforementioned, the formation of SO_2 during calcination of coal gangue is mainly governed by the transformation of pyrite. In oxygen-containing atmosphere, the transformation process of pyrite is complicated [20, 21], involving at least four reactions, as listed below.[20] The standard Gibbs free energies ($\Delta_r G^{\theta}$) of the reactions are listed in Table 2. It can be seen that the

$\Delta_r G^{\theta}$ of all reactions except the decomposition of pyrite (Eq. 2) gives a large negative value, indicating the relatively difficulty of the pyrite decomposition and strong possibilities of all the other reactions.

$FeS_2(s) \rightarrow FeS_x(s) + (1\text{-}0.5x)S_2(g)$ (2)

$S_2(g) + 2O_2(g) \rightarrow 2SO_2(g)$ (3)

$2FeS_x(s) + (1.5+2x)O_2(g) \rightarrow Fe_2O_3(s) + 2xSO_2(g)$ (4)

$2FeS_2(s) + 5.5O_2(g) \rightarrow Fe_2O_3(s) + 4SO_2(g)$ (5)

The ferrous sulfate and ferric sulfate may also form according to the following reactions:

$2FeS_2(s) + 7O_2(g) \rightarrow Fe_2(SO_4)_3(s) + SO_2(g)$ (6)

$FeS_2(s) + 3O_2(g) \rightarrow FeSO_4(s) + SO_2(g)$ (7)

To further elucidate the transformation of pyrite during calcination of coal gangue, the mineral phases in the coal gangue residues as well as pure pyrite after calcination were analyzed. The XRD patterns of residual ashes of CG1, CG2 and pyrite at 500 - 700 ^{o}C are shown in Fig. 6. It can be seen that the major mineral phase is hematite (Fe_2O_3) for both CG1 and CG2, which is in good agreement with the phase equilibrium diagram of iron oxides and oxygen presented by Darken and Gurry [22]. There is no indication that any FeS_x is formed while small amounts of ferric sulfate ($Fe_2(SO_4)_3$) or ferrous sulfate ($FeSO_4$) exist. The XRD pattern of pure pyrite calcined at 500 ^{o}C for 20 min (Fig. 6c) also manifests that no FeS_x is formed while both $Fe_2(SO_4)_3$ and $FeSO_4$ can be observed. A similar result was also obtained by Schorr et al. [23] In addition, the pyrite calcined at 600 ^{o}C and 700 ^{o}C also proved the generation of hematite.

Based on these observations, the reaction mechanism is proposed to be the direct oxidation of pyrite other than a two-step process (i.e. first decomposition and successive

oxidation), i.e., the pyrite is directly oxidized to form hematite according to reaction (4) via surface reaction. As the experiment was conducted under air atmosphere, the supply of oxygen is sufficient. At 500, 600 and 700 ^{o}C, the decomposition rates of pyrite may be lower than the oxidation rates. Therefore, pyrite undergoes direct oxidation. This mechanism is also favored by other investigators in the experiments of pyrite transformation under similar conditions [18, 24].

3.4. Kinetics analysis

The reaction rate *r* of SO_2 generation can be expressed as below [25],

$$r = \frac{dx}{dt} = k(T) f(x) \qquad (8)$$

where *x* is the fractional conversion, *k*(T) is the rate constant at the temperature *T*, and *f(x)* is the mechanism function. Alternatively, in terms of integral form, we obtain

$$F(x) = \int_0^x \frac{dx}{f(x)} = k(T)t = k_0 \exp(\frac{E}{RT})t \qquad (9)$$

By plotting the function *F(x)* against the time of reaction, the correlation coefficient can be calculated. An appropriate mechanism function could be estimated by comparing the linear relationships between different *F(x)* and *t*.

It shows that there is no single mechanism function that can conform with the experimental data across the whole range. However, some functions are in good agreements with the curves at different segments. The selected most probable mechanism functions under different conditions are shown in Table 3. As shown in Fig. 7, the experimental data of CG1 and CG2 at 500 ^{o}C, 600 ^{o}C and 700 ^{o}C were reasonably reproduced by a 3-D diffusion (Jander, *n*=1/2) model [26] at the initial stage of the reaction (Fig. 7a) and Jander model [26] at the following stage (Fig. 7b). For sample CG1 and CG2, the probable mechanisms are the same at different temperatures.

Many previous studies employed the shrinking core model to describe the direct oxidation of mineral pyrite [27-29], the model, however, is unable to reproduce the experimental results on coal gangue in this study. The difference may be attributed to the surrounding minerals of pyrite in coal gangue. As shown in Fig. 3, pyrite in coal gangue is embedded in the aluminosilicate, i.e., kaolinite and quartz, in separate or connected spherical aggregations. The general size of the aggregations is 30 to 50 μm. As the coal gangue samples employed in present study were sieved to 150 μm, pyrite in the coal gangue should be coated by kaolinite or quartz. The gas diffusion rate, i.e., the outward diffusion of formed SO_2, through the mineral layer is limited, which deviates from the shrinking core model.

According to equation (9), the intrinsic surface reaction rate *k(T)* can be obtained by the slope of the curves of *F(x)* versus *t* in Fig. 7. By plotting ln*k(T)* against *1/T* (shown in Fig. SI2), the activation energy *E* can thus be derived according to the following equation [25]:

$$\ln k(T) = \ln A - \frac{E}{RT} \quad (10)$$

The results of the intrinsic surface reaction rate *k(T)* and activation energy *E* are also listed in Table 3. The activation energy only slightly increased for CG1 at the later stage compared to the initial stage of the reaction, while it increased significantly for CG2, indicating the increase of diffusion resistance in CG2.

4. Conclusions

The SO_2 evolution and pyrite transformation during calcination of coal gangue was investigated. It can be found that sulfur in coal gangue was mainly in forms of pyrite whereas the content of organic sulfur was low, which is different from that of coal. The release of SO_2 in coal gangue was accelerated by the combustion of carbon content in coal gangue, which resulted in

lower start temperature and significantly higher release rate at 500 ^{o}C compared with pure pyrite. Pyrite was observed to undergo direct oxidation under the studied experimental conditions and the final product was majorly hematite. The evolution of SO_2 was initially followed the 3D diffusion models and correlated with Jander model in subsequent conversion, which showed no difference between two coal gangue. In addition, we also find that since coal gangue usually undergoes incomplete combustion, the carbon monoxide and other volatile matters generated during calcination may react with SO_2 and produce low-volatility acidic species in the presence of H_2O due to the dehydroxylation of clay minerals. These species may result in the corrosion of devices and various other operational problems. The result of the present study is significant to the further abatement of the SO_2 emission during coal gangue calcination.

Acknowledgments

This study was sponsored by The Common Development Fund of Beijing and the National Natural Science Foundation of China (51172003 and 51074009); The National High Technology Research and Development Program of China (863 Program, 2012AA06A114); The China National Key Technology R&D Program (2011BAB03B02 and 2013BAC14B07).

References

1. Z. F. Bian, X. X. Miao, S. G. Lei, S. E. Chen, W. F. Wang and S. Struthers, *Science*, 2012, **337**, 702-703.
2. M. Frias, R. V. de la Villa, M. I. S. de Rojas, C. Medina and A. J. Valdes, *J Am Ceram Soc*, 2012, **95**, 386-391.
3. C. C. Zhou, G. J. Liu, S. C. Wu and P. K. S. Lam, *Chemosphere*, 2014, **95**, 274-280.
4. X. Wang, C. Zhou, G. Liu and Z. Dong, *Analytical Letters*, 2013, **46**, 1962-1977.

5. Y. C. Zhao, J. Y. Zhang, C. L. Chou, Y. Li, Z. H. Wang, Y. T. Ge and C. G. Zheng, *Int J Coal Geol*, 2008, **73**, 52-62.
6. D. Nichol and N. P. Tovey, *Eng Geol*, 1998, **50**, 309-318.
7. F. D. Ardejani, B. J. Shokri, M. Bagheri and E. Soleimani, *Environ Earth Sci*, 2010, **61**, 1547-1560.
8. http://hzs.ndrc.gov.cn/newgzdt/201304/t20130412_536759.html. Accessed 13 June 2014.
9. F. R. Meng, J. L. Yu, A. Tahmasebi and Y. N. Han, *Energ Fuel*, 2013, **27**, 2923-2932.
10. D. X. Li, X. Y. Song, C. C. Gong and Z. H. Pan, *Cement Concrete Res*, 2006, **36**, 1752-1759.
11. C. C. Zhou, G. J. Liu, Z. C. Yan, T. Fang and R. W. Wang, *Fuel*, 2012, **97**, 644-650.
12. C. Zhou, G. Liu, S. Cheng, T. Fang and P. K. S. Lam, *Bioresource Technol*, 2014, **166**, 243-251.
13. Determination of Total Sulfur in Coal (GB/T 214), China, 2007.
14. Determination of Forms of Sulfur in Coal (GB/T 215), China, 2003.
15. S. Gornostayev, J. Harkki and O. Kerkkonen, *Fuel*, 2009, **88**, 2032-2036.
16. G. O'Brien, Y. Gu, B. J. I. Adair and B. Firth, *Miner Eng*, 2011, **24**, 1299-1304.
17. A. Á. B. Maia, R. S. Angélica, R. de Freitas Neves, H. Pöllmann, C. Straub and K. Saalwächter, *Appl Clay Sci*, 2014, **87**, 189-196.
18. J. P. Hansen, L. S. Jensen, S. Wedel and K. Dam-Johansen, *Ind Eng Chem Res*, 2003, **42**, 4290-4295.
19. S. L. Niu, K. H. Han and C. M. Lu, *Chem Eng J*, 2011, **168**, 255-261.
20. F. Paulik, J. Paulik and M. Arnold, *J Therm Anal*, 1982, **25**, 313-325.
21. G. L. Hu, K. Dam-Johansen, W. Stig and J. P. Hansen, *Prog Energ Combust*, 2006, **32**, 295-314.
22. L. Darken and R. Gurry, *J Am Chem Soc*, 1946, **68**, 798-816.
23. J. Schorr and J. Everhart, *J Am Ceram Soc*, 1969, **52**, 351-354.
24. G. M. Schwab and J. Philinis, *J Am Chem Soc*, 1947, **69**, 2588-2596.
25. S. Vyazovkin, A. K. Burnham, J. M. Criado, L. A. Perez-Maqueda, C. Popescu and N. Sbirrazzuoli, *Thermochim Acta*, 2011, **520**, 1-19.
26. P. Li, Q. B. Yu, H. Q. Xie, Q. Qin and K. Wang, *Energ Fuel*, 2013, **27**, 4810-4817.
27. N. Boyabat, A. K. Ozer, S. Bayrakceken and M. S. Gulaboglu, *Fuel Process Technol*, 2004, **85**, 179-188.
28. Y. Kajiwara, A. Sasaki and O. Matsubaya, *Geochem J*, 1981, **15**, 193-197.
29. I. C. Hoare, H. J. Hurst, W. I. Stuart and T. J. White, *J Chem Soc Farad T 1*, 1988, **84**, 3071-3077.

Table captions

Table 1 Proximate and Ultimate Analysis of Coal Gangue

Table 2 The Standard Gibbs Free Energies ($\Delta_r G^{\theta}$) of the Reactions

Table 3 The Kinetic Mechanism Functions and Parameters of Sulfur Dioxide Emission of Coal Gangue under Different Temperatures

Table 1 Proximate and Ultimate Analysis of Coal Gangue

	CG1	CG2
Proximate analysis (wt %)		
moisture, ad[a]	1.27	0.87
ash, d[b]	64.96	74.01
volatile matter, d	16.36	11.12
fixed carbon, d	18.68	14.88
Ultimate analysis (wt %)		
C, ad	20.37	15.78
H, ad	2.14	1.41
N, ad	0.60	0.55
Sulfur (d, wt %)		
total	1.84	0.91
organic	0.28	0.07
pyritic	1.45	0.81
sulfate	0.11	0.03
Major composition (wt %)		
SiO_2	31.8	41.2
Al_2O_3	28.1	26.3
Fe_2O_3	1.35	1.28
CaO	0.13	2.40
MgO	<0.1	0.27
K_2O	0.12	0.86
Na_2O	<0.1	0.13
TiO_2	0.96	0.85

[a] ad, air dried.

[b] d, dried.

Table 2 The Standard Gibbs Free Energies (Δ_rG^{θ}) of the Reactions

Reactions	Δ_rG^{θ} (kJ mol^{-1})		
	500 ^{o}C	600 ^{o}C	700 ^{o}C
$FeS_2(s) \rightarrow FeS_x(s) + (1\text{-}0.5x)S_2(g)$	34.259 (x=1)	20.311 (x=1)	6.383 (x=1)
$S_2(g) + 2O_2(g) \rightarrow 2SO_2(g)$	-610.785	-596.205	-581.660
$2FeS_x(s) + (1.5+2x)O_2(g) \rightarrow Fe_2O_3(s) + 2xSO_2(g)$	-1004.577 (x=1)	-976.188 (x=1)	-948.230 (x=1)
$2FeS_2(s) + 5.5O_2(g) \rightarrow Fe_2O_3(s) + 4SO_2(g)$	-1546.844	-1531.771	-1517.125
$2FeS_2(s) + 7O_2(g) \rightarrow Fe_2(SO_4)_3(s) + SO_2(g)$	-1776.886	-1680.175	-1584.124
$FeS_2(s) + 3O_2(g) \rightarrow FeSO_4(s) + SO_2(g)$	-823.684	-794.688	-765.978

Table 3 The Kinetic Mechanism Functions and Parameters of Sulfur Dioxide Emission of Coal Gangue under Different Temperatures

Reaction model		**M_1**				**M_2**			
		3-D diffusion (Jander)				Jander			
F(x)		$[1-(1-x)^{1/3}]^{1/2}$				$[1-(1-x)^{1/3}]^{2}$			
Sample	T/ ^{o}C	t/ min	R^2	k/ min^{-1}	E_a kJ/mol	t/ min	R^2	k/ min^{-1}	E_a kJ/mol
CG1	500	0-6	0.9458	0.03166	31	6-26	0.9963	0.03684	33
	600	0-5	0.9219	0.05755		5-12	0.9918	0.07436	
	700	0-3	0.9091	0.08506		3-8	0.9912	0.10588	
CG2	500	0-5	0.9674	0.03082	40	5-45	0.9807	0.00806	77
	600	0-3	0.9520	0.06069		3-16	0.9895	0.04424	
	700	0-2	0.9547	0.11126		2-9	0.9971	0.0921	

Figure captions

Fig. 1. The schematic diagram of the vertical tube furnace experimental system. 1-gas cylinder; 2-flow meter; 3-tube furnace; 4-thermocouple; 5-ceramic crucible; 6-gas analyzer; 7-computer.

Fig. 2. a) The XRD patterns of coal gangue. K-kaolinite ($Al_2Si_2O_5(OH)_4$), Q-quartz (SiO_2), C-calcite ($CaCO_3$), Py-pyrite(FeS_2); b) The Scanning Electron Microscopy Images of pyrite in coal gangue (CG2).

Fig. 3. The Thermogravimetric (TGA), Derivative Thermogravimetric (DTG) and Differential Scanning Calorimetric (DSC) curves of coal gangue and pyrite. The upward peaks on DSC curves represent exothermic reaction.

Fig. 4. The SO_2 release and conversion profiles of coal gangue and pure pyrite.

Fig. 5. Effect of temperature on SO_2 release and conversion: a) CG1, b) CG2 and c) pure pyrite.

Fig. 6. The XRD patterns of residual ash after calcined at different temperature.

Fig. 7. Diagram of different mechanism functions versus time.

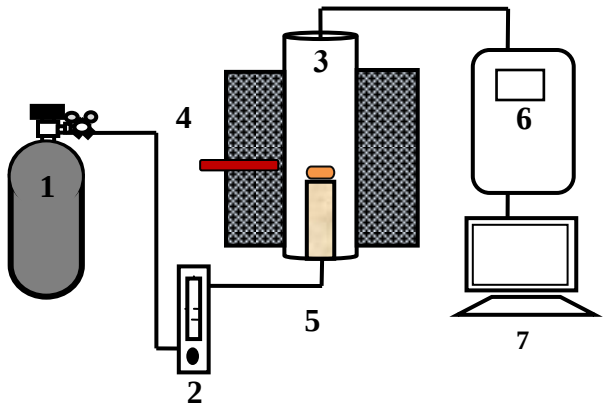

Fig. 1. The schematic diagram of the vertical tube furnace experimental system. 1-gas cylinder; 2-flow meter; 3-tube furnace; 4-thermocouple; 5-ceramic crucible; 6-gas analyzer; 7-computer.

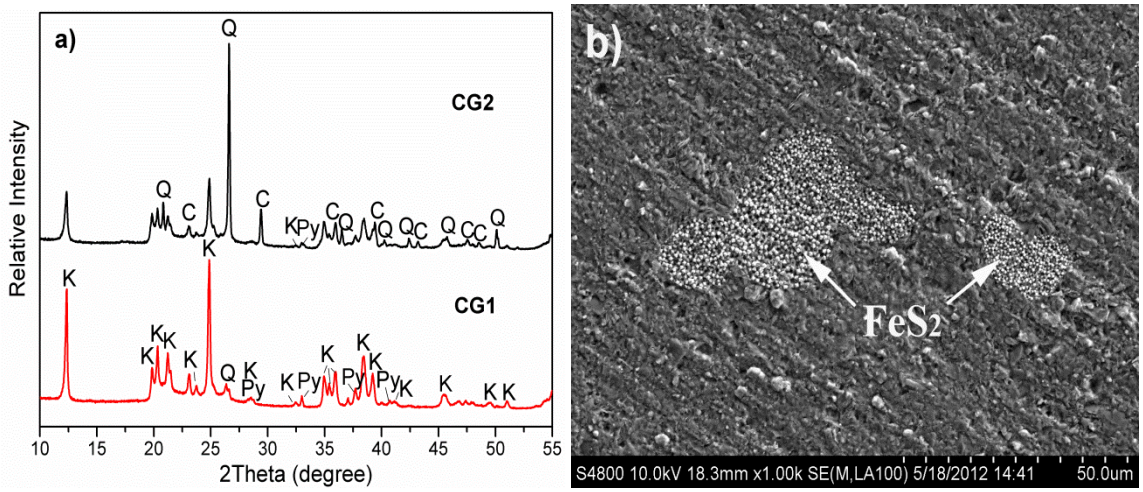

Fig. 2. a) The XRD patterns of coal gangue. K-kaolinite ($Al_2Si_2O_5(OH)_4$), Q-quartz (SiO_2), C-calcite ($CaCO_3$), Py-pyrite(FeS_2); b) The Scanning Electron Microscopy Images of pyrite in coal gangue (CG2).

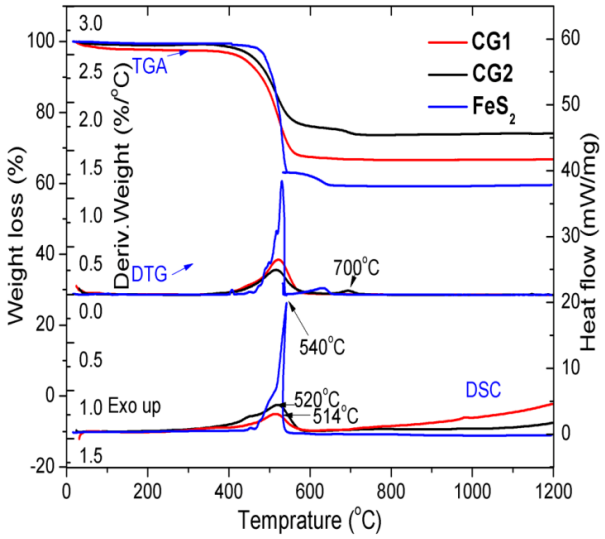

Fig. 3. The Thermogravimetric (TGA), Derivative Thermogravimetric (DTG) and Differential Scanning Calorimetric (DSC) curves of coal gangue and pyrite. The upward peaks on DSC curves represent exothermic reaction.

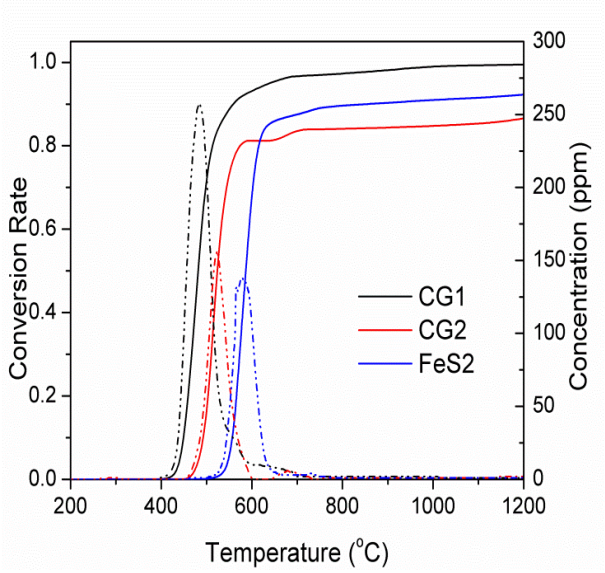

Fig. 4. The SO_2 release and conversion profiles of coal gangue and pure pyrite.

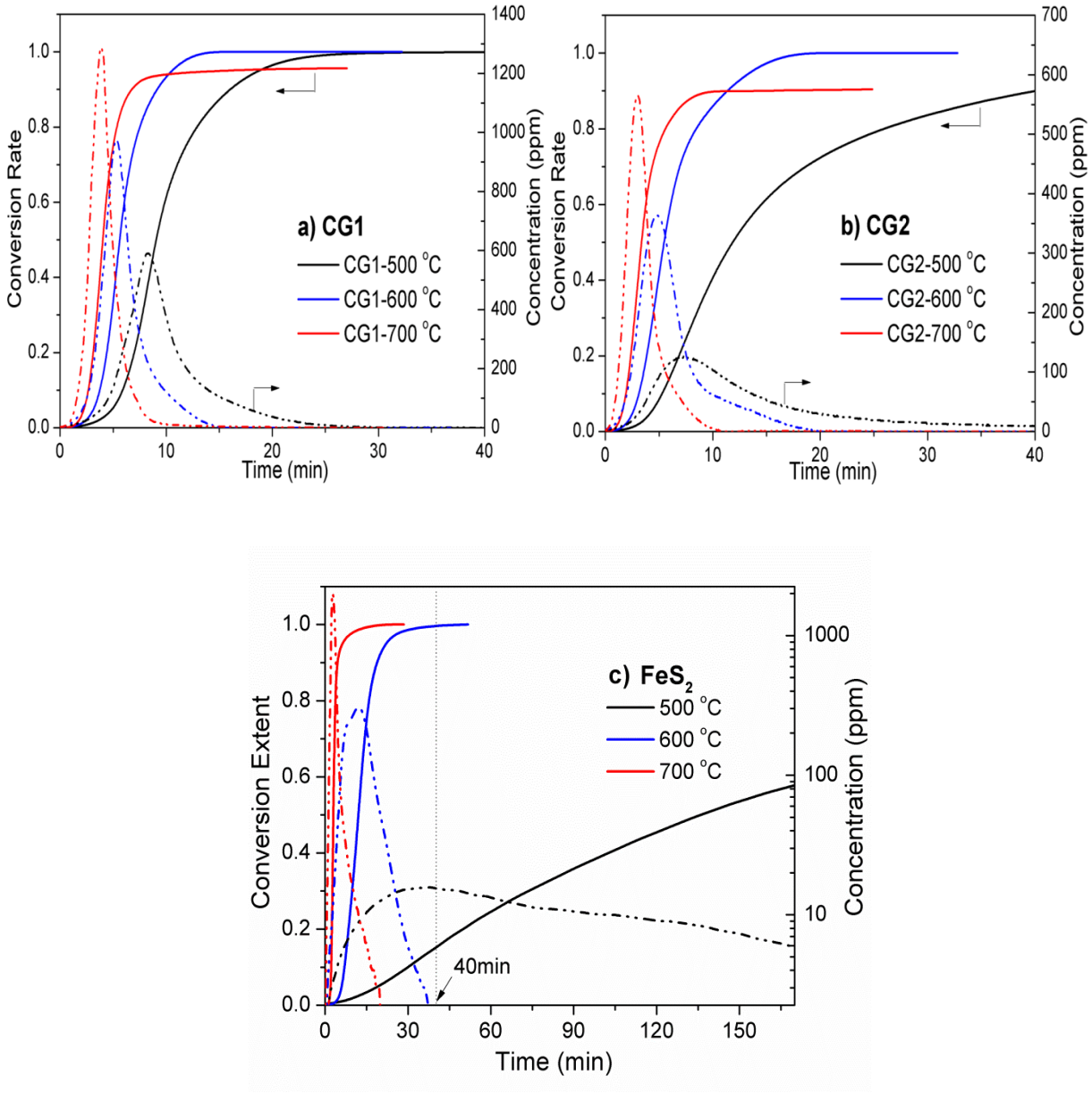

Fig. 5. Effect of temperature on SO_2 release rate and conversion of coal gangue as well as pure pyrite under isothermal conditions.

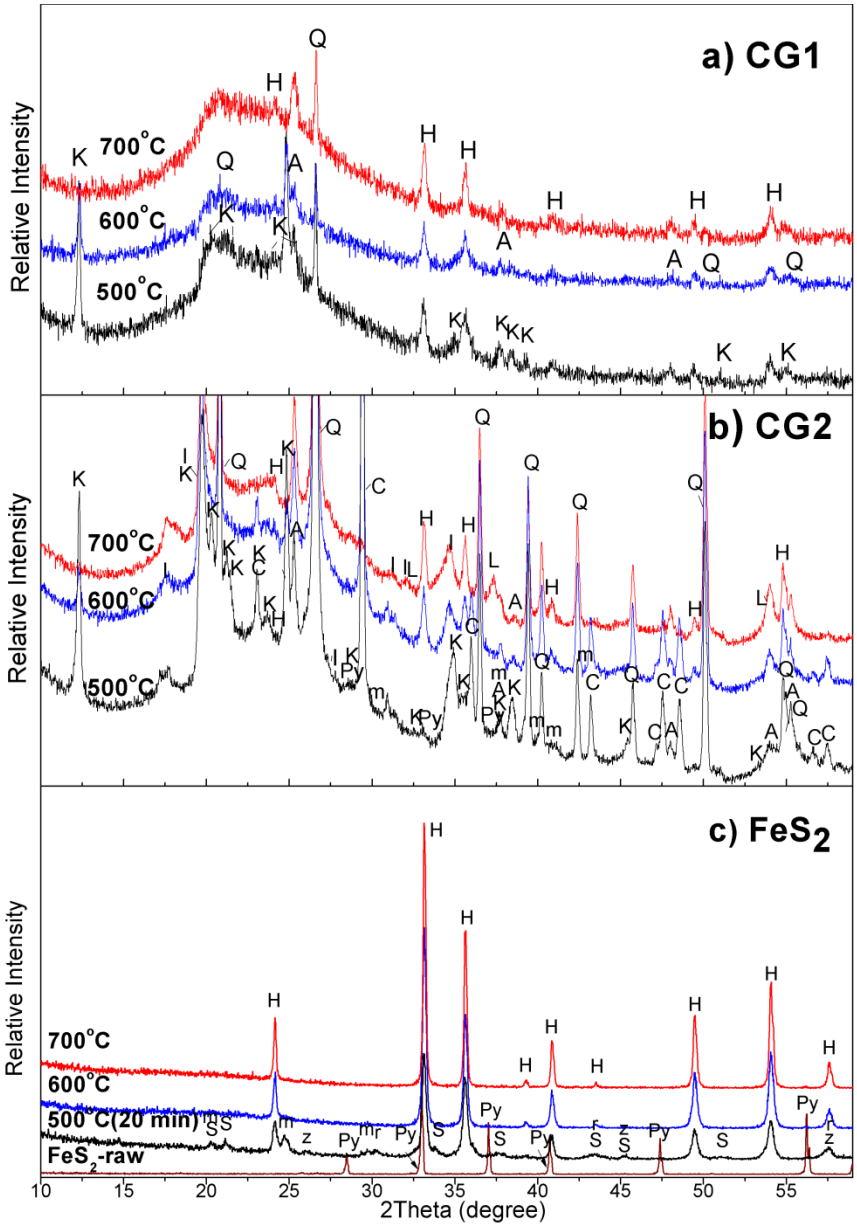

Fig. 6. The XRD patterns of residual ash after calcined at different temperatures. Py-pyrite (FeS_2), H-hematite (Fe_2O_3), m-mikasaite ($Fe_2(SO_4)_3$), S-iron sulfate ($FeSO_4$), z- Szomolnokite ($FeSO_4 \cdot H_2O$)

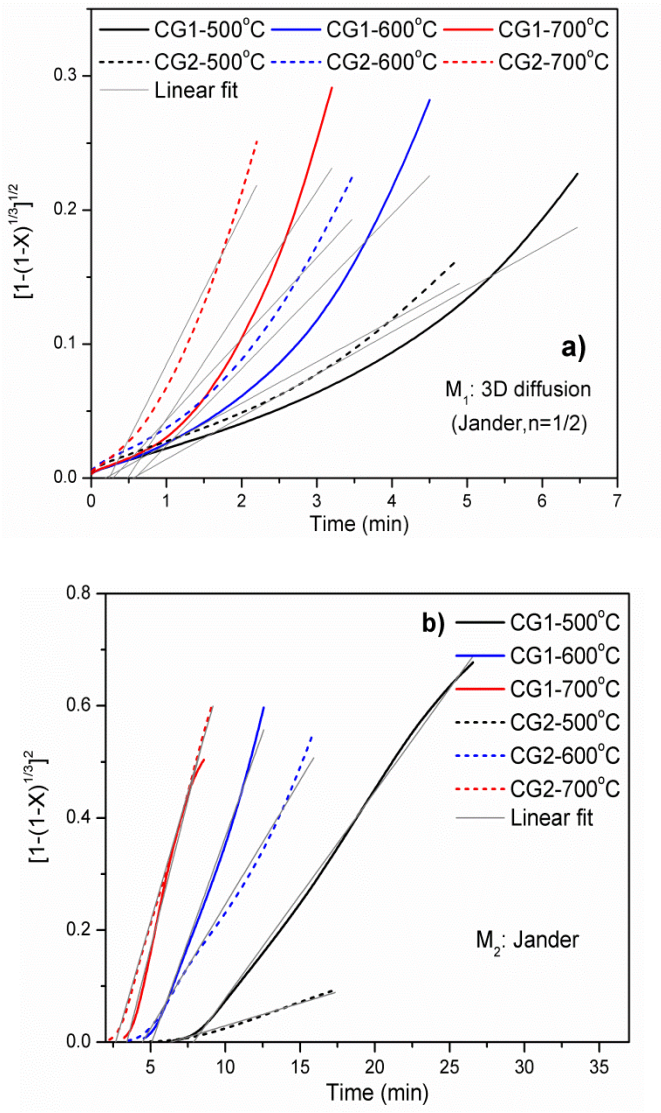

Fig. 7. Diagram of different mechanism functions versus time.